Role of a Conserved Salt Bridge between the PAS Core and the N-Terminal Domain in the Activation of the Photoreceptor Photoactive Yellow Protein

Daniel Hoersch,* Harald Otto,* Chandra P. Joshi,* Berthold Borucki,* Michael A. Cusanovich,† and Maarten P. Heyn*

*Biophysics Group, Department of Physics, Freie Universität Berlin, Berlin, Germany; and †Department of Biochemistry and Molecular Biophysics, University of Arizona, Tucson, Arizona

ABSTRACT The effect of ionic strength on the conformational equilibrium between the I_2 intermediate and the signaling state I_2' of the photoreceptor PYP and on the rate of recovery to the dark state were investigated by time-resolved absorption and fluorescence spectroscopy. With increasing salt concentration up to ~600 mM, the recovery rate k_3 decreases and the I_2/I_2' equilibrium (K) shifts in the direction of I_2'. At higher ionic strength both effects reverse. Experiments with mono-(KCl, NaBr) and divalent ($MgCl_2$, $MgSO_4$) salts show that the low salt effect depends on the ionic strength and not on the cation or anion species. These observations can be described over the entire ionic strength range by considering the activity coefficients of an interdomain salt bridge. At low ionic strength the activity coefficient decreases due to counterion screening whereas at high ionic strength binding of water by the salt leads to an increase in the activity coefficient. From the initial slopes of the plots of log k_3 and log K versus the square root of the ionic strength, the product of the charges of the interacting groups was found to be -1.3 ± 0.2, suggesting a monovalent ion pair. The conserved salt bridge K110/E12 connecting the β-sheet of the PAS core and the N-terminal domain is a prime candidate for this ion pair. To test this hypothesis, the mutants K110A and E12A were prepared. In K110A the salt dependence of the I_2/I_2' equilibrium was eliminated and of the recovery rate was greatly reduced below ~600 mM. Moreover, at low salt the recovery rate was six times slower than in wild-type. In E12A significant salt dependence remained, which is attributed to the formation of a novel salt bridge between K110 and E9. At high salt reversal occurs in both mutants suggesting that salting out stabilizes the more compact I_2 structure. However, chaotropic anions like SCN shift the I_2/I_2' equilibrium toward the partially unfolded I_2' form. The salt linkage K110/E12 stabilizes the photoreceptor in the inactive state in the dark and is broken in the light-induced formation of the signaling state, allowing the N-terminal domain to detach from the β-scaffold PAS core.

INTRODUCTION

PYP is a small cytoplasmic photoreceptor (14 kDa) from *Halorhodospira halophila* that is the structural prototype of the PAS domain family (1,2). *Halorhodospira halophila* is negatively phototactic in response to intense blue light with an action spectrum suggestive of PYP. The blue light absorption of PYP ($\lambda_{max} = 446$ nm) is due to its 4-hydroxycinnamoyl chromophore that is covalently bound via a thioester linkage to Cys-69. In the initial dark state the 7–8 double bond of the chromophore is *trans* and the chromophore is deprotonated. Rapid photoisomerization to the *cis* state (3) is followed by a cascade of dark reactions between various thermal intermediates leading back to the initial state (4). The main features of the photocycle of PYP, including absorption maxima, lifetimes, protonation changes, and equilibria, are shown in Fig.1 *C*. The first intermediate relevant for this article is I_1, which absorbs at 460 nm and still has a deprotonated chromophore. I_1 decays in several hundred microseconds to I_2, which has a protonated chromophore and absorbs around 370 nm (5–7). I_2 decays in ~2 ms to I_2', which is further blue-shifted to ~350 nm (5–7). Solution studies show that the formation of I_2' is associated with a global conformational change. Circular dichroism (8) and Fourier transform infrared (9,10) spectroscopy indicate a major change in secondary structure. NMR measurements suggest increased flexibility and disorder in the N-terminal domain (11,12). I_2' decays to the initial dark state P in several hundred milliseconds. This recovery transition is associated with reisomerization, chromophore deprotonation, and reversal of the structural change. It is likely that the longest lived intermediate I_2' with the largest structural change interacts transiently with a response regulator and should be identified with the signaling state. PYP is an excellent model system for studying the mechanism of PAS domain proteins, since high resolution x-ray structures are available for the dark state (13) and a number of photocycle intermediates (14,15). The solution structure has also been characterized by high resolution NMR in the dark (16) and in the light (11).

The initial light-induced structural perturbation is localized in the chromophore binding pocket on one side of the central β-sheet. The global structural change appears to involve

Submitted February 13, 2007, and accepted for publication May 2, 2007.

Address reprint requests to Maarten P. Heyn, Biophysics Group, Dept. of Physics, Freie Universität Berlin, Arnimallee 14, 14195 Berlin, Germany. Tel.: 49-30-83856160; Fax: 49-30-83856299; E-mail: heyn@physik.fu-berlin.de.

Abbreviations used: PAS domain, acronym formed from the names of the first three proteins recognized as sharing this sensory domain; PYP, photoactive yellow protein.

Editor: Janos K. Lanyi.

0006-3495/07/09/1687/13 $2.00

doi: 10.1529/biophysj.107.106633

mainly the other side of the β-scaffold, in particular the N-terminal domain. This segment of residues 1–28 forms a subdomain in the PYP structure that is packed against the central β-sheet. An important unresolved question is how the signal is transmitted across the central β-sheet. Attention has been called in this connection to the potential role of the interface between these domains in the formation of the signaling state (17,18).

The latter part of the photocycle, involving the intermediates I_1, I_2, and I_2', has been studied extensively (4,7,19–22). It was shown that the cycle is not unidirectional but includes back reactions and equilibria between intermediates (7,20–23). Of particular interest is the equilibrium between I_2 and the signaling state I_2', which involves the global conformational change. The first evidence for this dynamic equilibrium was obtained from double flash photoreversal measurements (24). This conformational equilibrium is pH dependent with a pK_a of ~6.3 with I_2' the main species above the pK_a (5–7). We found that over the pH range from 4.5 to 11.0 the recovery rate is proportional to the concentration of the I_2' intermediate (7,22).

The formation of the signaling state I_2' is associated with an increase in the radius of gyration (25) and exposure of a hydrophobic surface area (26), with hydrophobic dyes binding transiently to I_2' but not to I_2 (19). The NMR spectra of a photostationary mixture of I_2 and I_2' in solution showed structural disorder and exchange on the millisecond timescale (11), which were attributed to partial unfolding presumably in the I_2' state (12). Thus the rate constant for the return of I_2' to the initial dark state P can be viewed as a refolding rate constant. Its temperature dependence shows distinct non-Arrhenius behavior with a change in sign of the slope in log k against $1/T$ plots (26). Such a temperature dependence is typical for folding reactions and can be described satisfactorily by assuming that the reaction is associated with a large change in heat capacity (27). It has also been shown that over a wide pH and temperature range, the kinetics of refolding from the acid-denatured state of PYP, with the protonated chromophore in the *cis*-state, are the same as that of the photocycle recovery kinetics from I_2' to P (28). Thus, there is substantial evidence that the I_2 to I_2' and the I_2' to P transitions are associated with partial unfolding and refolding, respectively.

Fig. 1 *A* shows that the N-terminal domain of PYP is packed against the central β-sheet of the PAS core. Our working hypothesis is that, in the I_2 to I_2' transition, the N-terminal domain becomes detached and disordered, exposing the central β-sheet. We postulate further, that one of the major interactions between these two domains is the salt linkage between K110 (central β-sheet) and E12 (N-terminal domain) that is broken in the formation of I_2' and reformed in the I_2' to P transition (refolding). The space filling structure of Fig. 1 *B* shows that in the dark state the nitrogen of K110 and the oxygens of E12 are accessible from the surface.

Our working hypothesis is based on recent work where we showed that the I_1, I_2, and I_2' equilibria are strongly dependent

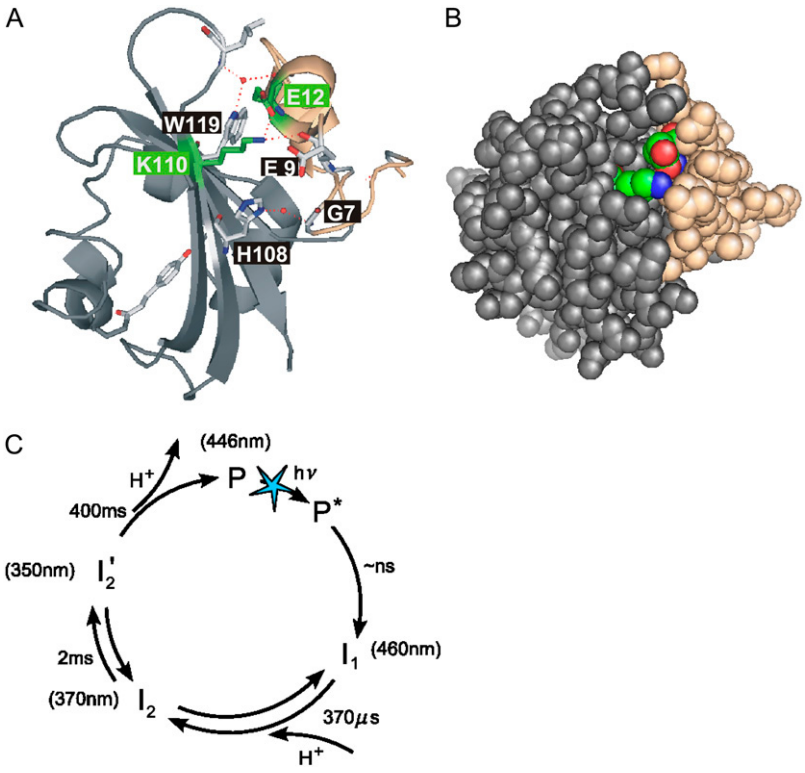

FIGURE 1 (*A*) View of the backbone structure of PYP with the N-terminal domain in the dark state on the right (*wheat color*) and the PAS core on the left (*gray color*) based on Protein Data Bank file 1NWZ (56). Lys-110 and Glu-12 are labeled in green. The side chain of K110 makes a salt bridge with E12 and a hydrogen bond with the backbone carbonyl of E9. In the mutant E12A an alternate salt bridge of K110 with the carboxyl of E9 is feasible. (*B*) Space filling view from the same direction as in panel *A*, showing that the charged groups of K110 and E12 are accessible from the surface. Figures generated using the program PyMol. (*C*) Simplified scheme of the photocycle of PYP from *Halorhodospira halophila*.

on the salt concentration in the mutant Y98Q (18). Analysis of the amplitude spectra derived from transient absorption spectroscopy indicated that salt had its primary effect on the I_2/I_2' equilibrium. Because the absorption spectra of these species were not available, it was not possible to quantify these effects further. It was concluded that salt shifts the I_2/I_2' equilibrium toward I_2' and that at very low salt the amount of light-induced signaling state is quite low. We argued that in the absence of salt, the salt linkage K110/E12 between the β-scaffold (K110) and the N-terminal domain (E12) keeps the photoreceptor in the inactive state (18). Salt-induced weakening of this electrostatic interaction (''ionic lock'') would allow the light-induced detachment of the N-terminal cap from the β-sheet and permit the global conformational change that is associated with the I_2 to I_2' transition (18). For wild-type, preliminary experiments indicated similar salt-induced effects on the I_1 and I_2/I_2' equilibria but these could not be analyzed in the absence of accurate absorption spectra for the I_2 and I_2' intermediates (18). In the meantime (5–7) these spectra became available allowing for the first time a quantitative analysis.

The ion pair K110/E12 (K/D in *Rb. capsulatus* and *Rb. sphaeroides*) is conserved in all known single domain PYP species, but is not present in the multidomain species Ppr and Ppd, which have enzymatic domains and photocycles that differ strongly from that of *Halorhodospira halophila* PYP (29,30). In LOV domain proteins a conserved K/E salt bridge keeps two domains together and may play an important role in the functional cycle (31,32).

The goals of the studies reported here were twofold. First, to show how the ionic strength affects the I_2/I_2' equilibrium and the recovery rate in wild-type and to investigate whether these salt effects can be explained on the basis of existing theories. Second, to identify the postulated ion pair with the salt bridge K110/E12 by investigating the properties of the mutants K110A and E12A.

Surprisingly little quantitative work has been done concerning the effect of ionic strength on the stability and rate of formation of salt bridges that link protein domains. Our analysis may thus be of more general interest, for example, for protein folding.

MATERIALS AND METHODS

Protein production and purification

H. halophila holo-PYP was produced by the use of the biosynthetic enzymes TAL and pCL and subsequently purified from *Escherichia coli* BL21 (DE3) as described (33). The mutagenesis was performed as described (34).

Transient absorption spectroscopy

Time-resolved absorption spectroscopy with 10–50 ns time resolution was performed as described (35). The wild-type spectra of the I_1, I_2, and I_2' intermediates at pH 7 were obtained in previous work (5,7,22). The corresponding intermediate spectra of the K110A and E12A mutants were determined at KCl concentrations of 20 mM and 1 M and pH values of 5.7 and 8 (data not shown). They were essentially the same as those of wild-type. Once these spectra are known, the time courses of the intermediate concentrations may be obtained from the transient absorbance changes $\Delta A(\lambda,t)$ by matrix inversion of the Lambert-Beer law (7,22).

Time-resolved fluorescence measurements

The decay of the fluorescence intensity of W119 after ps-excitation at 298 nm was measured by single photon counting as described (5). Background illumination from a light emitting diode emitting at 470 nm was used to generate a photostationary mixture of P and the I_2 and I_2' intermediates in the fluorescence cuvette (5). All spectroscopic measurements were performed at room temperature and in 10 mM Tris buffer.

Dependence of the recovery rate on ionic strength

As in our previous work (18) we consider that the K110/E12 salt linkage is broken in the formation of the I_2' intermediate. In the recovery reaction, this salt bridge reforms. The latter is an intramolecular reaction in which two oppositely charged groups interact to form the salt bridge. The salt dependence of the rate of this reaction can be modeled using standard concepts of physical chemistry, the primary kinetic salt effect (36,37). Two ions A and B with charges z_A and z_B react via a transition state X to P:

$$A^{z_A} + B^{z_B} \leftrightarrows X^{(z_A+z_B)} \rightarrow P, \tag{1}$$

in an aqueous solution of ionic strength

$$I = \frac{1}{2}\sum_i z_i^2 c_i. \tag{2}$$

The transition state X is not to be confused with the I_2 intermediate. Recalling that the activities (a_i) are the product of the concentrations c_i and the activity coefficients f_i, the rate of the reaction k is given by

$$k = k_0 \frac{f_A f_B}{f_x}, \tag{3}$$

where k_0 is the rate constant at ionic strength zero. The ionic strength dependence of the activity coefficient f_i is given by

$$-\log f_i = \frac{A z_i^2 \sqrt{I}}{1 + B\sqrt{I}} - CI. \tag{4}$$

The first term describes the electrostatic screening (Debye-Hückel). The second term describes the binding of water at high salt, which leads to a reduction in the effective concentration of water and an increase in the activity coefficient (37,38). A, B, and C are positive constants. Substitution of Eq. 4 in Eq. 3 leads to the well-known Eq. 5 (36,37):

$$\log k = \log k_0 + \frac{2 z_A z_B A\sqrt{I}}{1 + B\sqrt{I}} + CI. \tag{5}$$

The value of A at room temperature for aqueous solutions is 0.509 (37). It turns out that for our data $B \approx 0$. Equation 5 thus describes a parabola in the variable $\sqrt{I}$ with positive curvature and a minimum. A plot of log k against $\sqrt{I}$ at low ionic strength allows a determination of the product $z_A z_B$ of the charges that interact. In this case with K110 and E12 we expect $z_A z_B$ to equal -1 and initially log k should decrease linearly with $\sqrt{I}$. At high ionic strength the third term will dominate and log k should increase again.

Effect of ionic strength on the I_2/I_2' equilibrium

We consider that salt converts the ''closed/locked'' structure of I_2 to the ''open/unlocked'' structure of I_2'. ''Closed'' and ''open'' refer to structural

states with the N-terminal domain attached to or detached from the β-scaffold, respectively. ''Locked'' and ''unlocked'' refer to the presence or absence of the K110/E12 salt linkage. The true dissociation constant K_0' for the intramolecular equilibrium between the closed form AB (I_2) with f_{AB} and the open form A^+ B^- (I_2') with f_A, f_B is given by

$$K_0' = \frac{c_A c_B f_A f_B}{c_{AB} \; f_{AB}}, \tag{6}$$

with the true concentrations $c_A = c_B$ and c_{AB}, where $c_A + c_{AB} = c_0$. Introducing the normalized concentrations $[I_2'] \equiv c_A/c_0 = c_B/c_0$, and $[I_2] \equiv c_{AB}/c_0$ and the normalized dissociation constant $K_0 = K_0'/c_0$ we get

$$K \equiv K_0/F = [I_2']^2/[I_2], \tag{7}$$

where $F = (f_A f_B)\,/\,f_{AB}$. Consequently,

$$\log K = \log K_0 - \log F = \log K_0 - \frac{2 z_A z_B A\sqrt{I}}{1 + B\sqrt{I}} - CI. \tag{8}$$

Equation 8 describes a parabola in $\sqrt{I}$ with negative curvature and a maximum. Comparison of Eqs. 8 and 5 shows that apart from a vertical offset, these parabolas are mirror images. Note that changing the pH only affects this offset ($\log K_0$ in Eq. 8 and $\log k_0$ in Eq. 5), whereas the shape of the curves is pH independent. A plot of $\log K$ against $\sqrt{I}$ at low ionic strength allows a second independent determination of the charge product $z_A\, z_B$. With the sign of the expected charge product negative, the initial slope of $\log K$ against $\sqrt{I}$ should be positive. We note that the initial slopes of the plots of $\log K$ and $\log k$ against $\sqrt{I}$ differ by a factor of -1.

Effect of the I_2 / I_2' equilibrium on the apparent recovery rate k_{app}

We showed that the intermediates I_1, I_2, and I_2' are in equilibrium before they decay together to P (7,18,21,22). For the recovery to P (refolding) we have

$$\frac{dP}{dt} = \sum_{i=1}^{3} k_{iP} N_i(t), \tag{9}$$

where the sum over i extends over the three intermediates with time courses $N_i(t)$. Since the equilibration between these intermediates is rapid compared to the microscopic recovery rates k_{iP} (7,22), the intermediates decay with the same time courses

$$N_i(t) = n_{ieq}(N_0 - P(t)),$$

and Eq. 9 simplifies to

$$\frac{dP}{dt} = \left(\sum_{i=1}^{3} k_{iP}\, n_{ieq}\right)(N_o - P(t)), \tag{10}$$

where n_{ieq} is the fraction of the intermediates in the state i, and N_o is the total concentration of PYP. The apparent recovery rate k_{app} is thus given by

$$k_{app} = \sum_{i=1}^{3} k_{iP}\, n_{ieq}. \tag{11}$$

From the pH dependence of the recovery rate and the fractional intermediate equilibrium concentrations, we found that from pH 4.5 to 11.0 the rate of recovery k_{app} is proportional to the concentration of I_2' and that the return to P occurs via I_2' (7,22). For the apparent recovery rate constant we have therefore

$$k_{app} = k_3(I_2' \rightarrow P) n_{eq}(I_2'). \tag{12}$$

We assume that this relationship (Eq. 12) between k_{app} and $[I_2']$, which was derived from the pH dependence, remains valid for the salt dependence. Whereas the microscopic rate k_3 was pH independent (7,22), we will find that the salt data require that k_3 is salt dependent. We expect that the salt dependence of the microscopic rate k_3, calculated from the experimental values of k_{app} and n_{eq} (I_2') according to Eq. 12, can be fitted by Eq. 5.

RESULTS

The effect of ionic strength on photocycle kinetics and intermediate populations in wild-type

Fig. 2 *A* shows the dependence of the photocycle kinetics on KCl at pH 7.1 at the four wavelengths 350, 390, 440, and 490 nm and four salt concentrations. These wavelengths were selected since they are diagnostic for the I_2' and I_2 intermediates, the ground state depletion signal, and the I_1 intermediate, respectively. Measurements were performed at the following 14 KCl concentrations: 0, 3, 6, 10, 16, 26, 41, 65, 100, 160, 260, 410, 700, and 1600 mM. Using the time traces at these four wavelengths and the known intermediate spectra (7) the time courses of the intermediate populations were calculated as described (7,22). The only assumption made is that the intermediate spectra do not depend on the ionic strength. The intermediate time courses obtained in this way at four selected salt concentrations are shown in Fig. 2 *B*. The

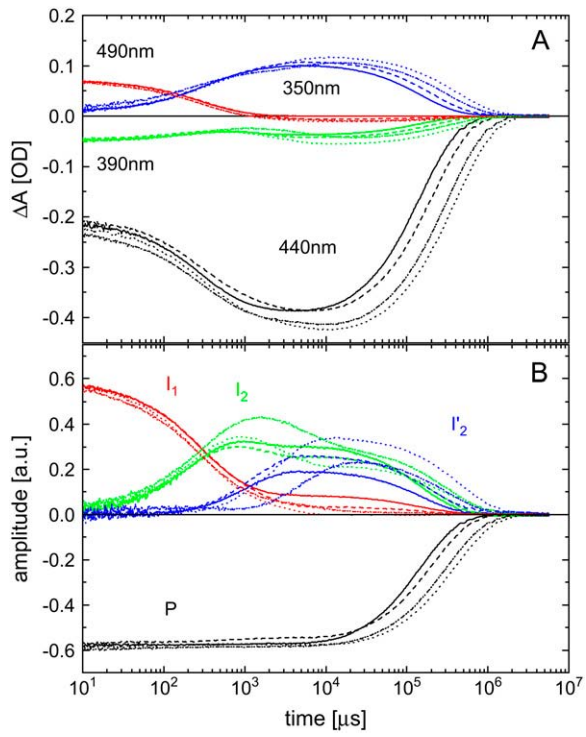

FIGURE 2 (*A*) Time traces of the transient absorbance changes at 350, 390, 440, and 490 nm of wild-type PYP at pH 7.1 and selected KCl concentrations of 6 (*solid line*), 100 (*dashed line*), 700 (*dotted line*), and 1600 (*dash-dotted line*) mM. (*B*) Time courses of the I_1, I_2, and I_2' populations derived from the data of panel *A* at the corresponding salt concentrations and the intermediate spectra of Borucki et al. (7). *P* is the depletion of the ground state.

traces labeled P represent the depletion and recovery of the ground state and remain almost constant in time until the recovery. The sum of the time courses of the I_1, I_2, I_2', and P populations is nearly zero for every ionic strength over the whole time range (not shown), showing the internal consistency of the data analysis. The results of Fig. 2 *B* indicate the presence of a strong salt effect on the I_1, I_2, and I_2' populations. In the time range where these three intermediates are in equilibrium (after the rise of I_2', ~2 ms), the concentration of I_2' increases with increasing ionic strength at the expense of I_1 and I_2. Above ~600 mM KCl, this effect is reversed. The rate constant for recovery k_{app} varies in the opposite direction, first decreasing and beyond 600 mM KCl increasing. We note that at 1.6 M KCl, the rise of I_2' is slower and the initial amount of I_2 larger than at the lower salt concentrations, which makes for a more pronounced initial I_2 peak. The dependence of K and of k_{app} on the ionic strength are presented in Fig. 3, *A* and *C*, respectively, for all the salt values. The equilibrium concentration values of I_2 and I_2' were taken from the time courses (Fig. 2 *B*) at 20 ms when the three intermediates are in equilibrium. K was calculated from these values according to $K = [I_2']^2/[I_2]$. To facilitate a comparison with the theoretical predictions of Eqs. 8 and 5, log K and log k_3 are plotted in Fig. 3, *A* and *C*, respectively, against the square root of the ionic strength (*solid square*). k_3 was calculated from k_{app} and $[I_2']$ using Eq. 12. The continuous curves are fits to the data according to Eqs. 8 and 5. These equations clearly provide an adequate fit over the entire ionic strength range; k_{app} and $[I_2']$ are not proportional over the salt range, but by making k_3 salt dependent, the relationship is retained (Eq. 12). We note that as expected from our model (Eqs. 8 and 5) the salt dependence of log K and log k_3 are indeed parabolic in $\sqrt{I}$ and approximate mirror images; k_3 initially decreases with increasing ionic strength since the attractive interaction between the oppositely charged groups of K110 and E12 is progressively reduced by the counterion clouds.

To obtain the value of the product $z_A z_B$ of the interacting charges, we used the data at low ionic strength where the contributions from the C-terms can be neglected and the linear terms in $\sqrt{I}$ of Eqs. 5 and 8 are sufficient. The low ionic strength data for KCl (*solid square*), $MgCl_2$ (*solid circle*), $MgSO_4$ (*solid triangle*) and NaBr (*star*) are replotted in Fig. 4, *A* and *B*, and fitted to the linear terms in $\sqrt{I}$ of Eqs. 5 and 8. From the common linear fits for log K and log k_3 of Fig. 4, *A* and *B*, we obtained slopes of 1.6 ± 0.2 and -1.1 ± 0.1, respectively, in good agreement with the prediction of Eqs. 5 and 8 that these slopes should differ by a factor of -1. According to Eqs. 8 and 5 the slope equals $-2z_A z_B A$ and $+2z_A z_B A$ for the log K and log k_3 plots, respectively. Using for the parameter A the value of 0.509 for aqueous solutions at room temperature (37), we obtain for the product of the charges of the reacting groups -1.5 ± 0.2 and -1.1 ± 0.1, respectively. Taking the error bars into account this result is consistent with -1, the value expected for a monovalent ion pair like

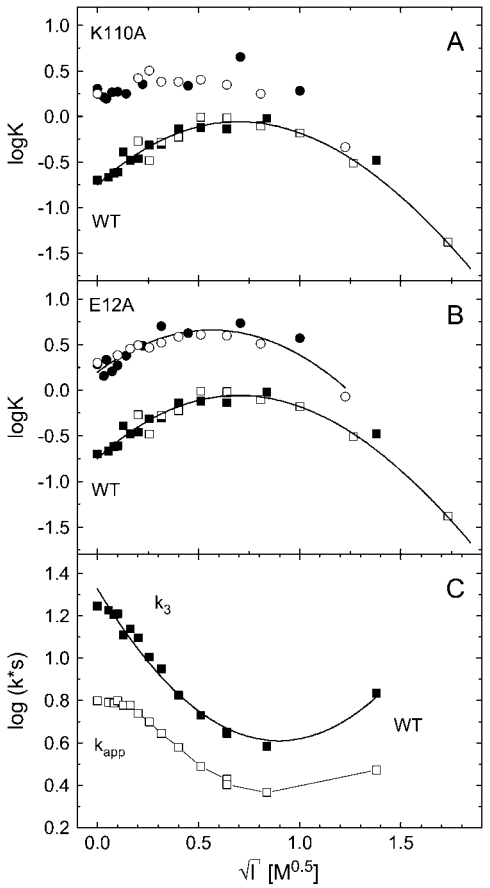

FIGURE 3 (*A*) Plot of log K against $\sqrt{I}$ for the KCl data for wild-type of Fig. 2 (■, transient absorbance, pH 7.1) together with the fit according to Eq. 8. The open squares are the results from the time-resolved fluorescence measurements of Fig.5 *B* (□, pH 8). *I* is the ionic strength. The results for the mutant K110A (derived from the data of Figs. 6 and 8) are marked by solid circle (transient absorbance, pH 8) and open circle (fluorescence, pH 7). To correct for the different pH values between the transient absorbance and fluorescence measurements a small offset was added to normalize the wild-type and K110A data at zero salt. (*B*) Plot of log K against $\sqrt{I}$ for the KCl data of E12A (●, transient absorbance, pH 8; ○, fluorescence, pH 7). The continuous curve is a fit with Eq. 8. (*C*) Plot of log k_3 (■) against $\sqrt{I}$ for the wild-type data of Fig. 2 together with the fit according to Eq. 5; k_{app} (□) is the experimental rate of recovery of the initial dark state P, and k_3 was calculated from k_{app} and $[I_2']$ using Eq. 12.

K/E. The choice of 0.509 for A is reasonable, since according to Fig. 1 *B* the K110/E12 salt linkage is accessible from the surface in the closed/locked state and the charged side chains of K110/E12 are expected to be hydrated in the unfolded open state I_2'. The linear dependence of log k_3 on $\sqrt{I}$ at low ionic strength is also known as the kinetic or primary salt effect (36).

For the divalent salts $MgCl_2$ and $MgSO_4$ the same ionic strength is reached at three and four times lower salt concentration as for KCl. Plotted as a function of $\sqrt{I}$ the results should fall on the same universal curves represented by Eqs. 5 and 8 and plotted in Fig. 3, *A* and *C*. We expect that at low ionic strength, when the ion-specific C-term in Eqs. 5 and 8

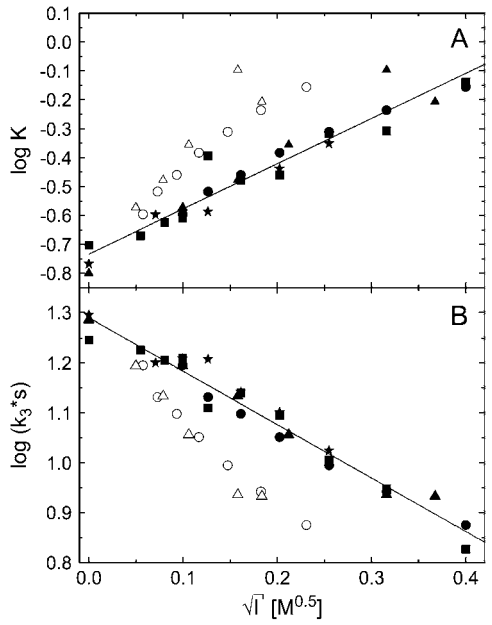

FIGURE 4 (*A*) Fit of the linear part of the ionic strength dependence of log *K* (Eq. 8) for wild-type PYP. ■, KCl; ●, $MgCl_2$; ▲, $MgSO_4$; ★, NaBr. The data of all four salts were used in a common fit. △, ○, $MgSO_4$ and $MgCl_2$ results plotted against the square root of the concentration, rather than the square root of the ionic strength. To correct for slightly different pH values between the measurements with different salts a small offset was added to normalize the data at zero salt. (*B*) Fit of the linear part of the ionic strength dependence of log k_3 with the second term of Eq. 5. ■, KCl; ●, $MgCl_2$; ▲, $MgSO_4$; ★, NaBr. The data of all four salts were used in a common fit. △, ○, $MgSO_4$ and $MgCl_2$ results plotted against the square root of the concentration, rather than the square root of the ionic strength.

can be neglected, the experimental effects are caused exclusively by unspecific Debye-Hückel screening of electrostatic interactions. Transient absorption experiments in the presence of various concentrations of $MgCl_2$ and $MgSO_4$ were carried out at pH 7.1 (data not shown) and analyzed as described above. The low ionic strength data for the I_2/I_2' equilibrium and k_3 are plotted in Fig. 4, *A* and *B*, as a function of $\sqrt{I}$ (*solid circle*, $MgCl_2$; *solid triangle*, $MgSO_4$) and of the square root of the $MgCl_2$ (*open circle*) and $MgSO_4$ (*open triangle*) concentrations. The data only fall on a straight line and agree with the results for the monovalent salts KCl (*solid square*) and NaBr (*star*) if plotted against $\sqrt{I}$ (Fig. 4, *A* and *B*, *solid circle* and *solid triangle*).

Effect of ionic strength on the amplitudes of the fluorescence from W119 in the I_2 and I_2' intermediates of wild-type

The fluorescence lifetime of the unique tryptophan W119 has widely different values of 0.18, 0.82, and 0.04 ns, respectively, for the P, I_2 and I_2' intermediates (5). This is due to the different extents of radiationless energy transfer between W119 and the chromophore in these states (5), which are a consequence of the different orientations of the chromophore transition dipole moments in these intermediates. Using background illumination from an LED emitting at 470 nm a photostationary mixture of P, I_2, and I_2' may be accumulated. In Otto et al. (5) the contributions of these three species to the fluorescence decay curves of the mixture were measured at various pH values and it was concluded that I_2 and I_2' are in a pH-dependent equilibrium with $pK_a \sim 6.3$. Here we performed similar experiments at fixed pH but at various salt concentrations to test whether the I_2/I_2' equilibrium depends on ionic strength. Fig. 5 *A* shows the intensity decay curves in the dark and in the presence of background illumination at pH 8 and 1.6 M KCl. The main differences are in the early and 1–2 ns parts of the decay curve where the formation of I_2' and I_2 leads to an increase in amplitude of the fastest and intermediate decay components. The slowest component with the lifetime of ~4.8 ns is due to a small contamination with apo-PYP (5). The intensities are plotted logarithmically in Fig. 5 *A*, which makes it difficult to recognize the magnitude of the difference in the fastest part of the decay curve. To magnify the effect and to focus only on the changes, the light minus dark differences are plotted in Fig. 5 *B* on a linear intensity scale. The measurements were performed at nine

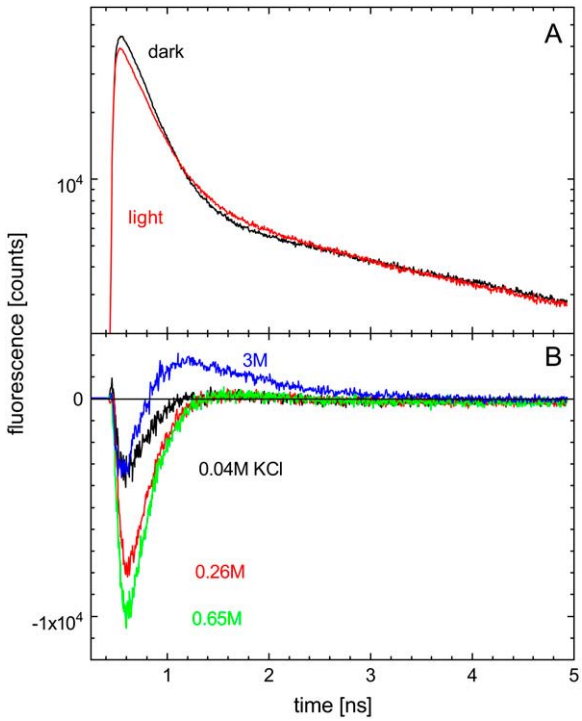

FIGURE 5 (*A*) Fluorescence intensity decay curves of W119 of wild-type PYP in P (*dark*) and in a photostationary mixture of P, I_2, and I_2' (*light*) accumulated by background illumination from an LED emitting at 470 nm. Excitation at 298 nm. Conditions, pH 8, 1.6 M KCl. (*B*) Light minus dark difference intensity decay at various concentrations of KCl as indicated. Note the linear intensity scale.

different KCl concentrations. For clarity only four traces are plotted in Fig. 5 *B*. The two decaying components in this light-dark difference, the fastest and the slowest, are due to I_2' and I_2, respectively. The rising component with the intermediate lifetime is due to P. The data in Fig. 5 *B* show that the amplitudes of the contributions of I_2' and I_2 are salt dependent. Normalizing the I_2 and I_2' amplitudes to the fraction cycling, the salt dependence of log *K* is plotted against $\sqrt{I}$ in Fig. 3 *A* (*open square*) to allow a comparison with the corresponding results from transient absorption spectroscopy (*solid square*). The salt dependence is qualitatively the same from both methods: at low ionic strength the I_2/I_2' equilibrium is shifted toward I_2', whereas at high ionic strength a reversal occurs. The fluorescence data thus provide strong and independent support for the results obtained from time-resolved transient absorption spectroscopy. We verified that the KCl concentration had no effect on the fluorescence decay of free tryptophan at pH 8 (measurements at 0 and 1.5 M KCl).

Effect of ionic strength on the photocycle kinetics and intermediate populations in the mutant K110A

The absorption spectrum of the mutant K110A is within experimental error identical to that of wild-type (data not shown). The salt dependence of the photocycle kinetics at pH 8 was investigated at the four wavelengths 340, 390, 450, and 490 nm, and 11 KCl concentrations between 0 and 1 M. For clarity data at only four salt concentrations are shown in Fig. 6 *A*. The salt dependence of the photocycle time traces at these wavelengths was much weaker than in wild-type (compare Fig. 6 *A* with Fig. 2 *A*). Using the wild-type spectra of I_1, I_2, and I_2' (7) these transient absorption data were transformed into the time courses of these intermediates as described in Materials and Methods. The wild-type spectra were used here, since the corresponding spectra for the mutant did not differ significantly (data not shown). The results are shown in Fig. 6 *B*, which should be compared with the corresponding results for wild-type in Fig. 2 *B*. Three conclusions can be drawn from this comparison. First, the salt effect on the I_2/I_2' equilibrium is much smaller in K110A than in wild-type. This is not due to a lack of I_2 at this pH. The time course of I_2 of Fig. 6 *B* shows that a considerable amount of this intermediate remains at pH 8. Second, the ionic strength effect on k_{app} is also much reduced with respect to wild-type below 600 mM KCl. At higher salt the reversal effect remains. Third, the cycle is considerably slower than in wild-type. For a quantitative comparison log *K* is plotted against $\sqrt{I}$ in Fig. 3 *A* for wild-type (*solid square*) and K110A (*solid circle*). Up to ~600 mM KCl the equilibrium concentrations of I_2 and I_2' in K110A barely change on the addition of KCl. The results for k_{app} are compared with those for wild-type in Fig. 7 *A*. Several differences are notable. The most important is that the salt dependence of k_{app} in K110A is much weaker than in wild-type, consistent with the smaller effect on the I_2/I_2' equilibrium population (Fig. 3 *A*). As a quantitative measure of the salt effect on the recovery rate, we may define the change in value of k_{app} between low salt and the minimum in Fig. 7 *A*. In units of s^{-1} we obtain 3.9 for wild-type and 0.2 for K110A. The second difference is that k_{app} is about six times smaller in K110A than in wild-type below 50 mM KCl. The fact that k_{app} is smaller in K110A is to be expected since the attractive electrostatic interaction between the charged groups of K110 and E12 that recombine in the recovery to P is absent in the mutant. One might also predict that complete screening of the charges of K110 and E12 in wild-type would reduce k_{app} to the value observed for the K110A mutant. Fig. 7 *A* shows that this is not quite the case, at least in part because the reversal above 600 mM KCl masks the effect.

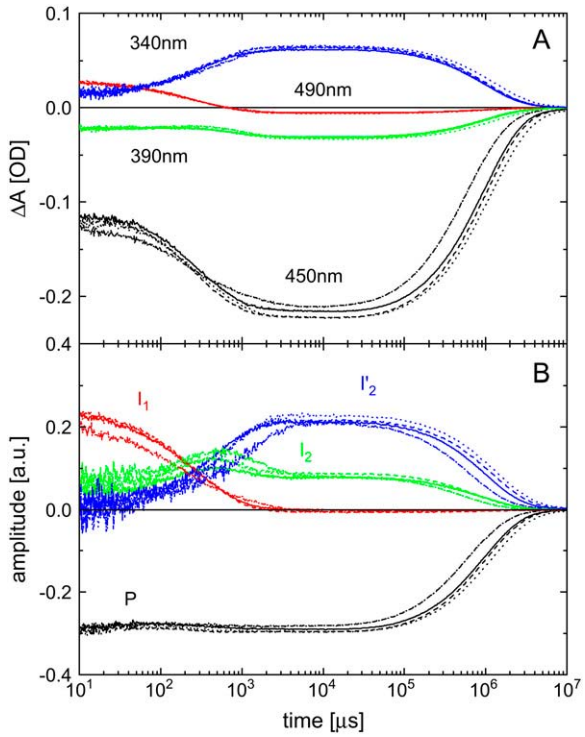

FIGURE 6 (*A*) Time traces of the transient absorbance changes at 340, 390, 450, and 490 nm of the mutant K110A at pH 8 and the four selected KCl concentrations of 0 (*solid line*), 20 (*dashed line*), 200 (*dotted line*), and 1000 (*dash-dotted line*) mM. (*B*) Time courses of the I_1, I_2, I_2', and P populations derived from the data of panel *A* at the corresponding salt concentrations. P represents the depletion and recovery of the ground state.

The I_2/I_2' equilibrium and recovery rate in wild-type are also strongly pH dependent with an apparent pK_a of ~6.3 (5,7,23). We measured the pH dependence of k_{app} and the I_2/I_2' equilibrium in the K110A mutant at 50 mM KCl and obtained a lower pK_a of ~5.8 (Fig. 7 *B*). At the same pH the equilibrium in K110A is shifted further in the direction of I_2' than in wild-type, as may be expected since the interdomain interaction is weaker. The titration results show that at pH 8 a considerable amount of the I_2 intermediate remains, in agreement with the time courses of Fig. 6 *B*.

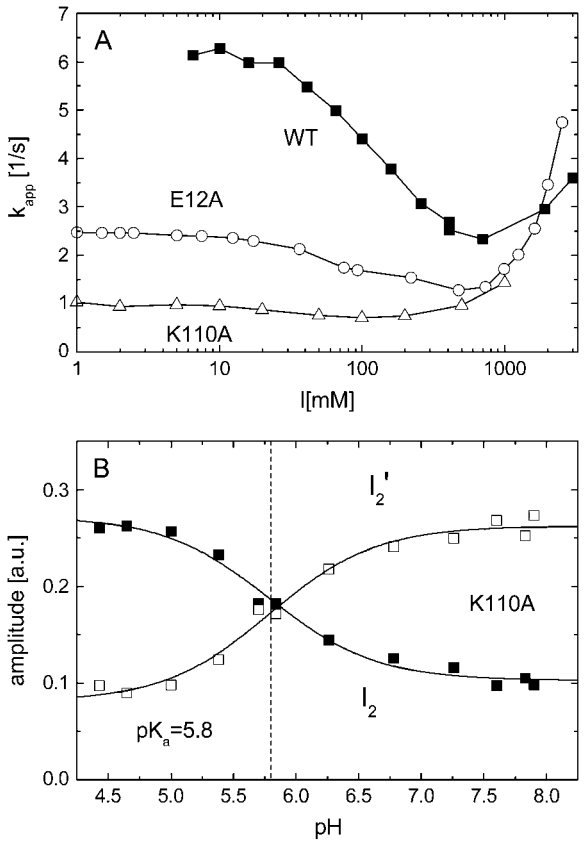

FIGURE 7 (*A*) Dependence of the experimental recovery rate k_{app} on the ionic strength (KCl) for wild-type (■, pH 7.1), E12A (○, pH 8), and K110A (△, pH 8). (*B*) pH dependence of the equilibrium concentrations of I_2 (■) and I_2' (□) in the mutant K110A. The solid curves are simultaneous fits with the Henderson-Hasselbalch equation with $pK_a = 5.8$ and $n = 1.0$. Conditions, 20 mM Tris, 50 mM KCl.

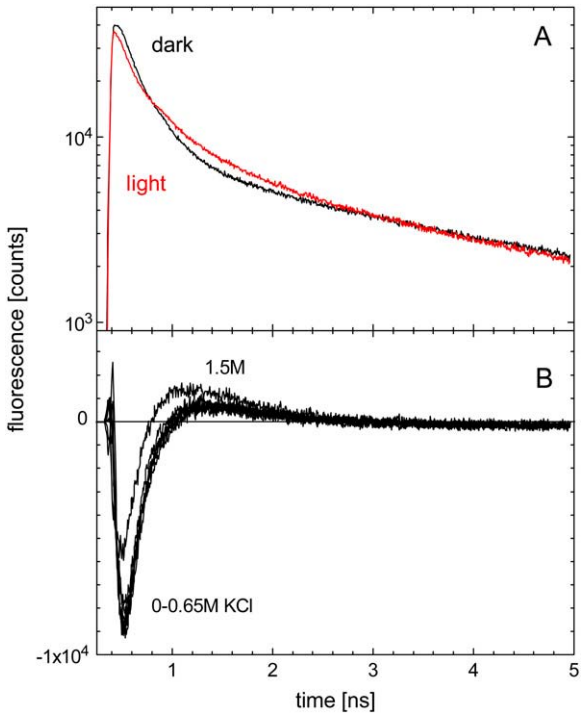

FIGURE 8 (*A*) Fluorescence intensity decay curves of W119 in the mutant K110A in the dark and in the presence of background illumination (*light*). Excitation at 298 nm. Conditions, pH 7, 1.5 M KCl. (*B*) Light minus dark difference intensity decays at various KCl concentrations as indicated.

Effect of ionic strength on the W119 fluorescence of I_2' in K110A

Further evidence for a strong reduction in the salt effect in this mutant was obtained from complementary fluorescence measurements. Fig. 8 *A* shows that at pH 7 in the presence of 1.5 M KCl and of background illumination, a substantial amount of both I_2 and I_2' accumulates. The light minus dark intensity difference is presented in panel *B* on a linear scale at a number of salt concentrations. Between 0 and 0.65 M KCl the amplitudes of the I_2 and I_2' contributions barely change. In spite of the presence of a considerable amount of I_2 (component with slowest time constant in Fig. 8 *B*), salt did not shift the equilibrium in the direction of I_2'. At 1.5 M KCl the amount of I_2' is reduced and that of I_2 is increased (Fig. 8 *B*). This is similar to the high salt reversal observed in wild-type, which apparently also occurs in the absence of the salt bridge. From these data the relative amount of I_2 and I_2' was calculated. The results for log *K* are plotted in Fig. 3 *A* (*open circle*) together with the corresponding results from flash spectroscopy (*solid circle*). There is good agreement between the results from these two different methods. Note that these fluorescence data for the K110A mutant were collected at pH 7, the same pH at which the wild-type flash data of Fig. 3 *A* were measured.

Effect of ionic strength on the photocycle kinetics of the mutant E12A

This mutation did not affect the wavelength of maximal absorbance of the chromophore. The recovery is slowed down with respect to wild-type by a factor of 2.5 at pH 8 and low salt (data not shown). Below ~500 mM KCl the salt dependence of k_{app} is weaker than in wild-type as shown by the data of Fig. 7 *A*. Using the same measure for the salt effect as defined above for K110A, we obtain from Fig. 7 *A* for E12A a value of 1.2, versus 3.9 for wild-type and 0.2 for K110A. At low ionic strength the salt dependence of the recovery rate is less than in wild-type but stronger than in K110A (Fig. 7 *A*). At high salt the apparent recovery rate increases. This is similar to the reversal in wild-type. The effect of salt on the I_2/I_2' equilibrium was measured as described by flash photolysis and fluorescence. The results are presented in Fig. 3 *B*, together with a fit according to Eq. 8. The data from both methods agree and show that the salt effect is similar though somewhat weaker than in wild-type. This is in line with the significant salt effect on k_{app}.

Effect of chaotropic anions

To gain a better understanding of the high salt reversal on the I_2/I_2' equilibrium, we tested the effect of the extreme chaotropes KSCN and $LiClO_4$. In Fig. 9 *A* the effect of potassium thiocyanate is compared with that of KCl. At low ionic strength thiocyanate behaves like other anions, i.e., it shifts the equilibrium toward I_2'. At high salt, however, no reversal occurs and the equilibrium is shifted even further toward I_2'. This in accordance with the corresponding observations on k_{app}, shown in Fig. 9 *B*, which likewise show no reversal at high ionic strength. Interestingly the slope of this salt dependence of k_{app} is much larger than for KCl. Similar results were obtained for ClO_4^-, another strongly chaotropic anion (data not shown).

DISCUSSION

In the formation of the signaling state I_2' of PYP a major structural change occurs that has been characterized as partial unfolding and that involves altering the interaction between the central β-sheet and the N-terminal cap. Indirect structural evidence suggests that these two domains detach in the I_2 to I_2' transition (25). Previously, we showed that salt shifts the equilibria between I_1, I_2, and I_2' in the mutant Y98Q toward

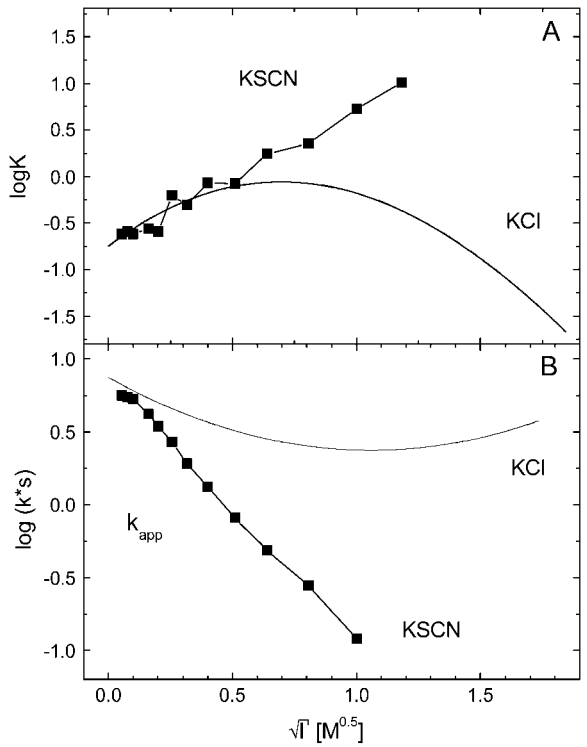

FIGURE 9 (*A*) Plot of log *K* against $\sqrt{I}$ for KSCN (■) obtained from transient absorbance data at pH 7. The fit for KCl from Fig. 3 *A* is shown for comparison. (*B*) Plot of log k_{app} against $\sqrt{I}$ for KSCN (■). Experimental conditions as in panel *A*. The fit for KCl from Fig. 3 *B* is shown for comparison.

I_2/I_2' and decreases the recovery rate (18). These effects at low salt were attributed to salt binding to the salt bridge K110/E12 in the I_2 to I_2' transition (18) with a binding constant of 115 mM. This interpretation of the data was tentative, since in the absence of accurate absorption spectra for I_2 and I_2' it was not possible to measure the salt effect on the I_2/I_2' equilibrium itself and since there was no direct evidence for such a role of the K110/E12 salt bridge. The only evidence was that the amplitude spectra at low and high salt indicated that the I_2 to I_2' transition was blocked in Y98Q at low salt (18). For wild-type, the existence of a salt effect on the $I_1/I_2/I_2'$ equilibria was demonstrated in Borucki et al. (18), but no systematic data were collected and in the absence of I_2 and I_2' spectra, the effect on the I_2/I_2' equilibrium could not be investigated. Here we show for the first time directly how salt affects the I_2/I_2' equilibrium and use the K110A and E12A mutants to elucidate the role of the K110/E12 salt bridge. The reversal at high salt was attributed to the salting out property of KCl, which stabilizes the compact and folded I_2 structure (18).

Based on the x-ray structure, the central β-sheet and the N-terminal cap interact by Coulomb, van der Waals, and hydrophobic interactions. Specific interactions involve the water-mediated hydrogen bonds between H108 and G7 as well as between W119 and E12, and the weak CH/π hydrogen bond between K123 and F6 (57). In addition there is the salt linkage between K110 and E12 (see Fig. 1). Residues E12, H108, K110, and W119 are highly conserved suggesting that they may play a role in the activation of PYP. The electrostatic interaction between K110 and E12 is just one of the contributions to the total interaction energy between these domains, but the short distance of 2.7 Å between the ε amino nitrogen of K110 and the carboxyl oxygen of E12 implies that it may make a substantial contribution. Screening of the charges of K110 and E12 by counterions or substitution of these charged residues by alanine may thus facilitate the conformational transition to the signaling state I_2' as well as slowing the recovery to P, in which this ion pair has to be reformed.

We tested these hypotheses by examining the effect of ionic strength on the I_2/I_2' equilibrium as well as on the rate of recovery k_{app} in wild-type and in the mutants K110A and E12A. Since the spectra of the I_2 and I_2' intermediates are now known (5–7), we can derive the time courses of their populations from the experimental ΔA (λ, t) traces at any ionic strength. Moreover, using the fact that the fluorescence lifetime of W119 has very different values in the I_2 and I_2' intermediates, the relative amount of these species may alternatively be obtained by measuring the time-resolved fluorescence decay curves in the presence of background illumination, as described (5).

The results from these two methods were in good agreement. Up to ~600 mM KCl the I_2/I_2' equilibrium in wild-type is shifted in the direction of I_2', and at higher ionic strength a reversal back to I_2 sets in. The dependence of the recovery rate on salt reflects the dependence of the I_2/I_2' equilibrium on

ionic strength: up to 600 mM a progressive slowing of the recovery, followed by acceleration above 600 mM. The experimental dependence of log K and log k_3 on $\sqrt{I}$ are described by two parabolas that are to a good approximation mirror images (see Fig. 3, *A* and *C*), as predicted by Eqs. 8 and 5. The good agreement between experiments and theory is unlikely to be fortuitous. Equations 5 and 8 are based on standard concepts from physical chemistry involving counterion screening of the charged groups at low salt and water binding and dehydration at high salt.

The slopes of the plots of log K and log k_3 against $\sqrt{I}$ at low ionic strength (Fig. 4, *A* and *B*) allowed us to determine the product of the charges that interact. From these two sets of independent measurements we obtained values of -1.5 ± 0.2 and -1.1 ± 0.1, which are in good agreement considering the errors. The average value is close to -1, the value expected for an ion pair like K110/E12. This is a crucial result. It shows that the charges that interact and are screened are of opposite sign and most likely $+1$ and -1. We note that the coefficient A in Eqs. 5 and 8 is not an adjustable parameter. The fact that the charge product $z_A\, z_B$ has this value strongly suggests that the model is applicable. The charge products from these two independent sets of measurements are in agreement thanks to the experimental fact that log k_3 decreases and log K increases with ionic strength. In other words the opposite slopes in Fig. 4, *A* and *B*, are essential. The internal consistency between the two sets of experimental data and Eqs. 5 and 8 is a further argument that the model and its underlying assumptions are correct.

To test whether the observed salt effects depend only on the ionic strength and not on the ion species, experiments were carried out with the 2:1 electrolyte $MgCl_2$ and the 2:2 electrolyte $MgSO_4$. As shown in Fig. 4, *A* and *B*, when plotted against $\sqrt{I}$ there is good agreement between the results for the monovalent salts (KCl and NaBr) and for $MgCl_2$ and $MgSO_4$. However, the agreement is lost, when the results are plotted against the square root of the salt concentration (Fig. 4, *A* and *B*). These observations lend further support for the idea that the effect at low ionic strength is due to unspecific counterion screening and does not depend on the cation or anion charge or species.

In the mutant K110A, the dependence of K and k_{app} on the ionic strength is virtually absent below 600 mM KCl (Figs. 3 *A* and 7 *A*). Moreover, k_{app} is smaller by a factor of six than in wild-type. These results strongly suggest that K110 is one of the residues that contribute to the salt bridge. PYP has many other charged groups besides K110 and E12, thus, it is not to be expected that removal of the K110/E12 salt bridge will lead to the complete disappearance of the ionic strength dependence. A residual effect is expected to remain. For the protein Fyn SH3, for example, it was recently shown that log k for folding is linear in $\sqrt{I}$, but with a positive slope (41). In this case no salt bridge was involved, but the sign was attributed to a cluster of negative surface charges (41). At high salt the reversal effect is still present in the mutant (Fig. 8 *B*).

For E12A a significant salt dependence of K and k_{app} was observed, which is similar to that of wild-type. Since the side chain of K110 also makes a hydrogen bond to the backbone carbonyl of E9 (see Fig. 1 *A*), replacement of K110 by alanine eliminates interactions of K110 with both E9 and E12. When E12 is replaced by alanine, however, the salt bridge is lost but the hydrogen bond between K110 and E9 would be expected to remain. More importantly the ε-amino group of K110 can now form a novel salt bridge with the carboxyl group of E9 (see Fig. 1 *A*), as we showed by energy minimization and model building. This requires some movement of the E9 side chain, which can occur without a steric clash. We attribute the observed salt dependence of the I_2/I_2' equilibrium and recovery rate in E12A to the presence of this new salt bridge.

Our result for the salt dependence of the recovery rate of the mutant K110A (Fig. 7 *A*) is consistent with those reported for the truncated PYP's T6 and T15 in which the first six or 15 N-terminal residues were removed by proteolytic digestion (17). For T6 (with the K110/E12 salt linkage presumably still intact) a minimum in the salt dependence of the recovery rate around 600 mM NaCl was observed as in wild-type. For T15 however (no salt bridge) the decrease of the recovery rate at low salt was absent, but the high salt reversal was still present. These T15 results are similar to our results for the K110A and E12A mutants reported in Fig. 7 *A*, which clearly indicate the reversal at 1 M KCl.

Two phases could be distinguished in the salt dependence for wild-type, the low salt phase due to screening and the reversal phase at high salt due to water binding to the salt. Eqs. 5 and 8 were based on the effects these phenomena have on the activity of the salt bridge K110A/E12A and thus appropriate for wild-type only. In the K110A and E12A mutants no effect would be expected to remain. The low salt screening effects on both the equilibrium and the recovery rates are indeed very much reduced as expected (Figs. 3 *A* and 7 *A*). A significant part of the high salt reversal phase remained, however, in the K110A and E12A mutants (Figs. 3, *A* and *B*, and 7 *A*) as in the T15 mutant (17). At high concentrations salt will affect the water structure and lead to salting out, whether the K110/E12 salt bridge is present or not. Salt increases the surface tension of water and thereby increases the free energy of cavity formation (42). In this way salt leads to the salting out of nonpolar groups (42). Since the I_2 to I_2' conformational transition is associated with an expansion (25) and exposure of a hydrophobic surface patch (26,19), high salt is expected to favor the compact and folded structure of the I_2 intermediate. Salting out will thus also shift the I_2/I_2' equilibrium back in the direction of I_2. We attribute the reversal effects in the mutants at high salt to these salting out effects. The third terms in Eqs. 5 and 8 for wild-type thus contain also salting out contributions, for which a linear dependence on the salt concentration is expected (41,42).

At high salt specific anion effects are expected to occur. Anions are ordered according to the strength of these effects

in the Hofmeister series (42). Our results with kosmotropic anions like Cl^- and SO_4^- showed that these favor the compact folded I_2 intermediate. For the strongly chaotropic anions SCN^- and ClO_4^- we found the opposite effect (Fig. 9 *A*): these anions shifted the I_2/I_2' equilibrium toward the unfolded form I_2', which has a larger radius of gyration. Extreme chaotropes like SCN^- also affect the initial dark state of PYP, shifting the ground state equilibrium in wild-type and the mutant Y42F toward a population with a protonated chromophore, which is less stabile and resembles the photocycle intermediate I_2' (43–45).

Taken together our results strongly suggest that the salt bridge K110/E12 plays a key role in keeping PYP in the inactive form in the dark and that this salt bridge needs to be broken on light-induced activation. The I_2/I_2' equilibrium may be compared to the M_I/M_{II} equilibrium in the photoreceptor rhodopsin, where high salt also favors the signaling state, M_{II}. It has been proposed that an ionic lock involving the conserved motif ERY of helix 3 and E247 of helix 6 holds these helices together in the dark (46). In M_{II}, these helices move apart (47,48), and this conformational change is a universal feature of G-protein coupled receptors (49), which share a common mechanism of activation (50). In the case of PYP our data strongly suggest that the N-terminal domain detaches from the β-scaffold of the PAS core in I_2', but direct structural evidence that these domains move apart is still lacking.

A change in domain interactions also plays a significant role in the activation of another PAS domain protein, the LOV2 domain of phototropin. High resolution solution structures were determined for the dark and the activated state (51,52). In this photoreceptor a light-induced distortion of the central β-sheet leads to dissociation of the C-terminal J_α helix from the PAS core and activation of the kinase activity (51,52). It seems that in PYP an analogous change in domain-domain interaction occurs in the formation of the signaling state but involving the detachment of the N-terminal cap from the central β-sheet. However, no salt bridge contributes to the domain-domain interaction in LOV2 (52).

Few experimental results are available on the effect of ionic strength on the rate of protein folding. However, with hen lysozyme the slowest folding rate constant ($\sim 1\ s^{-1}$) slowed with increasing NaCl concentration and displayed the same linear dependence of log k on $\sqrt{I}$ as observed here with PYP, i.e., with a negative slope (39). It was concluded that this slow phase of the folding is associated with the formation of a specific attractive ionic interaction (39). T4 lysozyme has an interdomain interaction that involves hinge-bending and the disruption of an interdomain salt bridge (40). In the open conformation the stabilizing salt bridge between E22 and R137, which links the two domains in the closed conformation, is broken and the distance between the charged groups increases to >17 Å (40). It seems likely that, as observed here for PYP, the formation of the closed form and the salt bridge is slowed by counterion screening of the Coulomb attraction.

It is of interest to compare our observations for a salt bridge between two protein domains with those for the related problem of the electrostatic interaction between two proteins. With oppositely charged interacting domains the association rate constant k_{as} and the equilibrium constant K decreased with ionic strength for the thrombin-hirudin and the barnase-barstar complexes (53–55) in the same way as observed here for PYP below 600 mM KCl. Changing the charge product of the two proteins by mutagenesis of charged residues in the interface region led to qualitative agreement with models with linear terms in $\sqrt{I}$ as in Eqs. 5 and 8 (53–55). This is similar to our observation with the K110A mutant of PYP. We note that in the case of the thrombin-hirudin complex plots of log K and log k_{as} against $\sqrt{I}$ showed clear curvature (55), which in the case of PYP could be described by the term proportional to I in Eqs. 5 and 8. In the work on the barnase-barstar complex an equation was proposed for log k_{as} which included only the linear term in $\sqrt{I}$ of Eq. 5 (54). For ionic strength below 100 mM the agreement was good, but curvature was observed here as well at higher salt concentration, which may well be accounted for by a term proportional to I as in Eq. 5.

To our knowledge an analysis of the salt dependence of a protein conformational equilibrium (I_2/I_2') and of a recovery (refolding) rate constant based on Eqs. 5 and 8 has not been reported. In protein folding the formation of interdomain salt bridges plays a significant role and the salt dependence of the stability of these salt bridges is likely of importance. The conceptual framework presented here may thus be applicable to related problems concerning the ionic strength dependence of protein structure and dynamics.

We thank Elsa Chan for making the K110A and E12A mutants.

This work was financially supported by grants from the National Institutes of Health (GM 66126 to M.A.C.) and the Deutsche Forschungsgemeinschaft (He 1382/14-1 to M.P.H. and H.O.).

REFERENCES

1. Cusanovich, M. A., and T. E. Meyer. 2003. Photoactive yellow protein: a prototypic PAS domain sensory protein and development of a common signaling mechanism. *Biochemistry.* 42:4759–4770.
2. Taylor, B. L., and I. B. Zhulin. 1999. PAS domains: internal sensors of oxygen, redox potential, and light. *Microbiol. Mol. Biol. Rev.* 63: 479–506.
3. Heyne, K., O. F. Mohammed, A. Usman, J. Dreya, E. T. J. Nibbering, and M. A. Cusanovich. 2005. Structural evolution of the chromophore in the primary stages of the trans/cis isomerization in photoactive yellow protein. *J. Am. Chem. Soc.* 127:18100–18106.
4. Hoff, W. D., I. H. M. van Stokkum, H.-J. van Ramesdonk, M. E. van Brederode, A. M. Brouwer, J. C. Fitch, T. E. Meyer, R. van Grondelle, and K. J. Hellingwerf. 1994. Measurement and global analysis of the absorbance changes in the photocycle of the photoactive yellow protein from Ectothiorhodospira halophila. *Biophys. J.* 67:1691–1705.
5. Otto, H., D. Hoersch, T. E. Meyer, M. A. Cusanovich, and M. P. Heyn. 2005. Time-resolved single tryptophan fluorescence in photoactive yellow protein monitors changes in the chromophore structure during the photocycle via energy transfer. *Biochemistry.* 44:16804–16816.
6. Shimizu, N., Y. Imamoto, M. Harigai, H. Kamikubo, Y. Yamazaki, and M. Kataoka. 2006. pH-dependent equilibrium between long lived near-UV

intermediates of photoactive yellow protein. *J. Biol. Chem.* 281:4318–4325.

7. Borucki, B., C. P. Joshi, H. Otto, M. A. Cusanovich, and M. P. Heyn. 2006. The transient accumulation of the signaling state of photoactive yellow protein is controlled by the external pH. *Biophys. J.* 91:2991–3001.
8. Lee, B.-C., P. A. Croonquist, T. R. Sosnick, and W. D. Hoff. 2001. PAS domain receptor photoactive yellow protein is converted to a molten globule state upon activation. *J. Biol. Chem.* 276:20821–20823.
9. Xie, A., L. Kelemen, J. Hendriks, B. J. White, K. J. Hellingwerf, and W. D. Hoff. 2001. Formation of a new buried charge drives a large-amplitude protein quake in photoreceptor activation. *Biochemistry.* 40: 1510–1517.
10. Brudler, R., R. Rammelsberg, T. T. Woo, E. D. Getzoff, and K. Gerwert. 2001. Structure of the I_1 early intermediate of photoactive yellow protein by FTIR spectroscopy. *Nat. Struct. Biol.* 8:265–270.
11. Rubinstenn, G., G. W. Vuister, F. A. A. Mulder, P. E. Düx, R. Boelens, K. J. Hellingwerf, and R. Kaptein. 1998. Structural and dynamic changes of photoactive yellow protein during its photocycle in solution. *Nat. Struct. Biol.* 5:568–570.
12. Craven, C. J., N. M. Derix, J. Hendriks, R. Boelens, K. J. Hellingwerf, and R. Kaptein. 2000. Probing the nature of the blue-shifted intermediate of photoactive yellow protein in solution by NMR: hydrogen-deuterium exchange data and pH studies. *Biochemistry.* 39:14392–14399.
13. Borgstahl, G. E. O., D. R. Williams, and E. D. Getzoff. 1995. 1.4 Å structure of photoactive yellow protein, a cytosolic photoreceptor: unusual fold, active site and chromophore. *Biochemistry.* 34:6278–6287.
14. Genick, U. K., G. E. Borgstahl, K. Ng, Z. Ren, C. Pradervand, P. M. Burke, V. Srajer, T. Y. Teng, W. Schildkamp, D. E. McRee, K. Moffat, and E. D. Getzoff. 1997. Structure of a protein photocycle intermediate by millisecond time-resolved crystallography. *Science.* 275:1471–1475.
15. Ihee, H., S. Rajagopal, V. Šrajer, R. Pahl, S. Anderson, M. Schmidt, F. Schotte, P. A. Anfinrud, M. Wulff, and K. Moffat. 2005. Visualizing reaction pathways in photoactive yellow protein from nanoseconds to seconds. *Proc. Natl. Acad. Sci. USA.* 102:7145–7150.
16. Dux, P., G. Rubinstenn, G. W. Vuister, R. Boelens, F. A. A. Mulder, K. Hard, W. D. Hoff, A. R. Kroon, W. Crielaard, K. J. Hellingwerf, and R. Kaptein. 1998. Solution structure and backbone dynamics of the photoactive yellow protein. *Biochemistry.* 37:12689–12699.
17. Harigai, M., Y. Imamoto, H. Kamikubo, Y. Yamazaki, and M. Kataoka. 2003. Role of an N-terminal loop in the secondary structural change of photoactive yellow protein. *Biochemistry.* 42:13893–13900.
18. Borucki, B., J. A. Kyndt, C. P. Joshi, H. Otto, T. E. Meyer, M. A. Cusanovich, and M. P. Heyn. 2005. Effect of salt and pH on the activation of photoactive yellow protein and gateway mutants Y98Q and Y98F. *Biochemistry.* 44:13650–13663.
19. Borucki, B., S. Devanathan, H. Otto, M. A. Cusanovich, G. Tollin, and M. P. Heyn. 2002. Kinetics of proton uptake and dye binding by photoactive yellow protein in wildtype and in the E46Q and E46A mutants. *Biochemistry.* 41:10026–10037.
20. Hendriks, J., I. H. M. van Stokkum, and K. J. Hellingwerf. 2003. Deuterium isotope effects in the photocycle transitions of the photoactive yellow protein. *Biophys. J.* 84:1180–1191.
21. Borucki, B., H. Otto, C. P. Joshi, C. Gasperi, M. A. Cusanovich, S. Devanathan, G. Tollin, and M. P. Heyn. 2003. pH dependence of the photocycle kinetics of the E46Q mutant of photoactive yellow protein: protonation equilibrium between the I_1 and I_2 intermediates, chromophore deprotonation by hydroxyl uptake, and protonation relaxation in the dark state. *Biochemistry.* 42:8780–8790.
22. Joshi, C. P., B. Borucki, H. Otto, T. E. Meyer, M. A. Cusanovich, and M. P. Heyn. 2006. Photocycle and photoreversal of photoactive yellow protein at alkaline pH: kinetics, intermediates and equilibria. *Biochemistry.* 45:7057–7068.
23. Imamoto, Y., M. Harigai, and M. Kataoka. 2004. Direct observation of the pH-dependent equilibrium between L-like and M intermediates of photoactive yellow protein. *FEBS Lett.* 577:75–80.
24. Joshi, C. P., B. Borucki, H. Otto, T. E. Meyer, M. A. Cusanovich, and M. P. Heyn. 2005. Photoreversal kinetics of the I_1 and I_2 intermediates in the photocycle of photoactive yellow protein by double flash experiments with variable time delay. *Biochemistry.* 44:656–665.
25. Imamoto, Y., H. Kamikubo, M. Harigai, N. Shimizu, and M. Kataoka. 2002. Light-induced global conformational change of photoactive yellow protein in solution. *Biochemistry.* 41:13595–13601.
26. Meyer, T. E., G. Tollin, J. H. Hazzard, and M. A. Cusanovich. 1989. Photoactive yellow protein from the purple phototrophic bacterium *Ectothiorhodospira halophila*. Quantum yield of photobleaching and effects of temperature, alcohols, glycerol and sucrose on kinetics of photobleaching and recovery. *Biophys. J.* 56:559–564.
27. Van Brederode, M., W. D. Hoff, I. H. M. Van Stokkum, M.-L. Groot, and K. J. Hellingwerf. 1996. Protein folding thermodynamics applied to the photocycle of the photoactive yellow protein. *Biophys. J.* 71: 365–380.
28. Lee, B.-C., P. A. Croonquist, and W. D. Hoff. 2001. Mimic of photocycle by a protein folding reaction in photoactive yellow protein. *J. Biol. Chem.* 276:44481–44487.
29. Jiang, Z. Y., L. R. Swem, B. G. Rushing, S. Devanathan, G. Tollin, and C. E. Bauer. 1999. Bacterial photoreceptor with similarity to photoactive yellow protein and plant phytochromes. *Science.* 285:406–409.
30. Kyndt, J. A., J. C. Fitch, T. E. Meyer, and M. A. Cusanovich. 2005. Thermochromatium tepidum photoactive yellow protein/bacteriophytochrome/diguanylate cyclase Ppd.: characterization of the PYP domain. *Biochemistry.* 44:4755–4764.
31. Crosson, S., S. Rajagopal, and K. Moffat. 2003. The LOV domain family: photoresponsive signaling modules coupled to diverse output domains. *Biochemistry.* 42:2–10.
32. Losi, A., E. Ghiraldelli, S. Jansen, and W. Gärtner. 2005. Mutational effects on protein structural changes and interdomain interactions in the blue-light sensing LOV protein YtvA. *Photochem. Photobiol.* 81: 1145–1152.
33. Kyndt, J. A., F. Vanrobaeys, J. C. Fitch, B. V. Devreese, T. E. Meyer, M. A. Cusanovich, and J. J. Van Beeumen. 2003. Heterologous production of *Halorhodospira halophila* holo-photoactive yellow protein through tandem expression of the postulated biosynthetic genes. *Biochemistry.* 42:965–970.
34. Kyndt, J. A., J. K. Hurley, B. Devreese, T. E. Meyer, M. A. Cusanovich, G. Tollin, and J. J. Van Beeumen. 2004. Rhodobacter capsulatus photoactive yellow protein: genetic context, spectral and kinetics characterization, and mutagenesis. *Biochemistry.* 43:1809–1820.
35. Borucki, B., H. Otto, and M. P. Heyn. 1999. Reorientation of the retinylidene chromophore in the K, L, and M intermediates of bacteriorhodopsin from time-resolved linear dichroism: resolving kinetically and spectrally overlapping intermediates of chromoproteins. *J. Phys. Chem. B.* 103:6371–6383.
36. Atkins, P. W. 1998. Physical Chemistry. Oxford University Press, Oxford, UK.
37. Bockris, J. O'M., and A.K.N. Reddy. 1998. Modern Electrochemistry, Vol. 1, 2nd Ed. Plenum Press, New York.
38. Stokes, R. H., and R. A. Robinson. 1948. Ionic hydration and activity in electrolyte solutions. *J. Am. Chem. Soc.* 70:1870–1878.
39. Itzhaki, L. S., P. A. Evans, C. M. Dobson, and S. E. Radford. 1994. Tertiary interactions in the folding pathway of hen lysozyme: kinetic studies using fluorescence probes. *Biochemistry.* 33:5212–5220.
40. Sinha, N., S. Kumar, and R. Nussinov. 2001. Interdomain interactions in hinge-bending transitions. *Structure.* 9:1165–1181.
41. de los Rios, M. A., and K. W. Plaxco. 2005. Apparent Debye-Hückel electrostatic effects in the folding of a simple, single domain protein. *Biochemistry.* 44:1243–1250.
42. Baldwin, R. L. 1996. How Hofmeister ion interactions affect protein stability. *Biophys. J.* 71:2056–2063.
43. Brudler, R., T. E. Meyer, U. K. Genick, S. Devanathan, T. T. Woo, D. P. Millar, K. Gerwert, M. A. Cusanovich, G. Tollin, and E. D.

Getzoff. 2000. Coupling of hydrogen bonding to chromophore conformation and function in photoactive yellow protein. *Biochemistry.* 39: 13478–13486.

44. Meyer, T. E., S. Devanathan, T. Woo, E. D. Getzoff, G. Tollin, and M. A. Cusanovich. 2003. Site specific mutations provide new insight into the origin of pH effects and alternative spectral forms in the photoactive yellow protein of *Halorhodospira halophila*. *Biochemistry.* 42:3319–3325.
45. El-Mashtoly, S. F., M. Unno, M. Kumauchi, N. Hamada, K. Fujiwara, J. Sasaki, Y. Imamoto, M. Kataoka, F. Tokunaga, and S. Yamauchi. 2004. Resonance Raman spectroscopy reveals the origin of an intermediate wavelength form in photoactive yellow protein. *Biochemistry.* 43:2279–2287.
46. Vogel, R., and F. Siebert. 2002. Conformation and stability of α-helical membrane proteins. 1. Influence of salts on conformational equilibria between active and inactive states of rhodopsin. *Biochemistry.* 41:3529–3535.
47. Farrens, D. L., C. Altenbach, K. Yang, W. L. Hubbell, and H. G. Khorana. 1996. Requirement of rigid-body motion of transmembrane helices for light activation of rhodopsin. *Science.* 274:768–770.
48. Sheikh, S. P., T. A. Zvyaga, O. Lichtarge, T. P. Sakmar, and H. R. Bourne. 1996. Rhodopsin activation blocked by metal-ion-binding sites linking transmembrane helices C and F. *Nature.* 383:347–350.
49. Ghadouni, P., J. J. Steenhuis, D. L. Farrens, and B. K. Kobilka. 2001. Agonist-induced conformational changes in the G-protein-coupling domain of the β2 adrenergic receptor. *Proc. Natl. Acad. Sci. USA.* 98:5997–6002.
50. Ballesteros, J. A., A. D. Jensen, G. Liapakis, S. G. Rasmussen, L. Shi, U. Gether, and J. A. Javitch. 2001. Activation of the β_2 adrenergic receptor involves disruption of an ionic lock between the cytoplasmic ends of transmembrane segments 3 and 6. *J. Biol. Chem.* 276:27171–27177.
51. Harper, S. M., L. C. Neil, and K. H. Gardner. 2003. Structural basis of a phototropin light switch. *Science.* 301:1541–1544.
52. Harper, S. M., J. M. Christie, and K. H. Gardner. 2004. Disruption of the LOV-J_α helix interaction activates phototropin kinase activity. *Biochemistry.* 43:16184–16192.
53. Schreiber, G., and A. R. Fersht. 1996. Rapid, electrostatically assisted association of proteins. *Nat. Struct. Biol.* 3:427–431.
54. Vijayakumar, M., K.-Y. Wong, G. Schreiber, A. R. Fersht, A. Szabo, and H.-X. Zhou. 1998. Electrostatic enhancement of diffusion-controlled protein-protein association: comparison of theory and experiment on barnase and barstar. *J. Mol. Biol.* 278:1015–1024.
55. Stone, S. R., S. Dennis, and J. Hofsteenge. 1989. Quantitative evaluation of the contribution of ionic interactions to the formation of the thrombin-hirudin complex. *Biochemistry.* 28:6857–6863.
56. Getzoff, E. D., K. N. Gutwin, and U. K. Genick. 2003. Anticipatory active-site motions and chromophore distortion prime photoreceptor PYP for light activation. *Nat. Struct. Biol.* 10:663–668.
57. Harigai, M., M. Kataoka, and Y. Imamoto. 2006. A single CH/π weak hydrogen bond governs stability and the photocycle of the photoactive yellow protein. *J. Am. Chem. Soc.* 128:10646–10647.